Thermo-Structural FEA Validation of a Cryogenic LN2 Propelled Pressure Vessel Under Combined Thermal and Internal Pressure Loading

A Computational Study Validating Orozco et al. (2025)

Independent Research Project

SolidWorks Simulation | Sequential Thermal-Structural Coupling

1. Introduction

Cryogenic storage vessels are critical components in liquid propulsion systems, industrial gas handling, and emerging hydrogen energy infrastructure. Such vessels contain fluids at temperatures far below ambient, generating large temperature gradients across their walls. When a structure is constrained against the free thermal contraction that these gradients induce, substantial internal stresses develop independently of any mechanical pressure load. The interaction between this constrained thermal contraction and the internal pressure that the vessel must simultaneously contain defines the thermo-structural design problem.

Orozco, Ramirez Zamora, Hossain and Choudhuri (2025), publishing in Aerospace, presented a coupled finite element analysis of the propellant tanks used in the Centennial Restartable Liquid Oxygen-Liquid Methane Engine (CROME) developed at the University of Texas at El Paso. Their study evaluated spherical stainless steel tanks storing liquid nitrogen, liquid oxygen, and liquid methane at 200 and 400 psi. They reported that the maximum von Mises stress consistently occurred at the nozzle-shell junction, that thermal loading rather than internal pressure was the dominant contributor to stress, and that the junction region should be reinforced in future designs.

The objective of the present work is to independently reproduce the thermo-structural modelling methodology of the reference study using SolidWorks Simulation, to validate its central findings concerning the location and magnitude of peak stress and the dominance of thermal loading, and to perform a bounded parametric study of the junction geometry, the stored fluid, and the operating pressure.

The work does not claim novel theory; its value lies in independent validation of a published result through a separate solver and an independently constructed model.

2. Methodology

2.1 Geometry

The vessel was modelled as a spherical shell of 910 mm inner diameter and 7 mm uniform wall thickness, corresponding to an outer diameter of 924 mm. Two coaxial cylindrical nozzles of 150 mm bore and 170 mm projection were positioned at the top and bottom poles, each terminating in a flat bolting flange. The solid was generated by a revolved thin feature about the central axis, producing the hollow shell directly, with the nozzle bores cut to communicate with the internal cavity. The model was constructed in SolidWorks 2024.

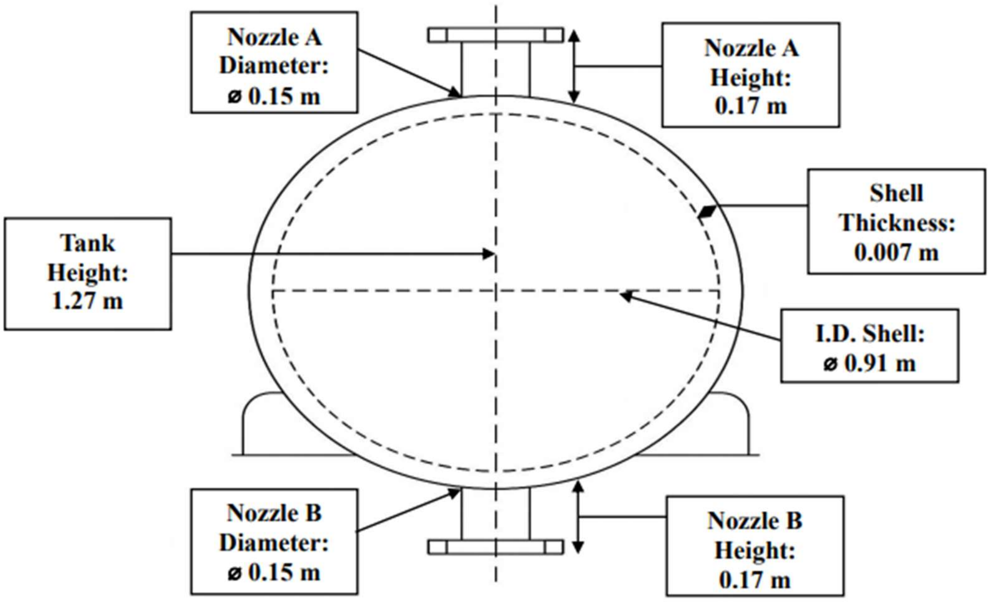

Figure 2. Geometry of the Cryogenic Vessel according to Orozco et al; this was not followed exactly.

2.2 Material

AISI 316 stainless steel was assigned to the entire body. The principal properties used were an elastic modulus of 193 GPa, a Poisson ratio of 0.27, and a coefficient of thermal expansion of 1.6 by ten to the minus five per degree Celsius. Consistent with the reference study, the ultimate tensile strength of 1,170 MPa, representing the enhanced strength of the alloy at cryogenic temperature, was used as the basis for the factor of safety calculation.

2.3 Boundary Conditions and Loading

A sequentially coupled thermal-to-structural procedure was employed. A steady-state thermal study was first solved to establish the temperature field. The internal surfaces of the shell and nozzle bores were held at the saturation temperature of the stored fluid, namely -165 degrees Celsius for liquid nitrogen at 200 psi, while the external surfaces were held at the ambient temperature of 26.7 degrees Celsius. This produced a through-wall gradient of 191.7 degrees. The resulting nodal temperature field was then imported into a static structural study as a thermal load, with the stress-free reference temperature set to 20 degrees Celsius. Internal pressure of 1.379 MPa (200 psi) was applied to the internal surfaces, acting outward. Both nozzle flanges were fully fixed, reproducing the constrained boundary condition of the reference study.

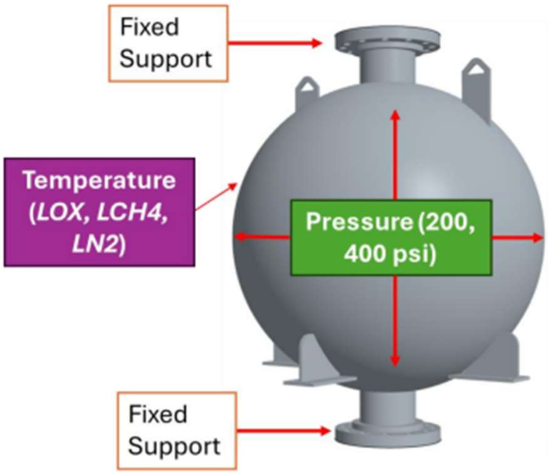

Figure 3. Thermo-structural model boundary & initial conditions according to Orozco et al; these were followed exactly.

Table 1. Model parameters and boundary conditions.

Parameter	Value	Source
Sphere inner diameter	910 mm	Reference geometry
Wall thickness	7 mm	Reference geometry
Nozzle bore / projection	150 mm / 170 mm	Reference geometry
Material	AISI 316 stainless steel	Reference study
Elastic modulus	193 GPa	Material library
Thermal expansion coeff.	1.6 x 10^-5 /degC	Material library
Inner wall temperature	-165 degC (LN2, 200 psi)	Reference Table 1
Outer wall temperature	26.7 degC (ambient)	Reference study
Internal pressure	1.379 MPa (200 psi)	Reference Table 1
Reference (stress-free) temp.	20 degC	Standard assumption
Constraint	Both flanges fixed	Reference study

2.4 Mesh

A curvature-based tetrahedral mesh was applied, with local refinement in the junction region where stress gradients are steepest. Mesh density was increased and the analysis repeated to confirm that the reported peak stress was stable with respect to further refinement.

3. Results and Discussion

3.1 Thermal Field

The steady-state thermal study produced a smooth gradient through the wall, with the internal surface at 108 K (-165 degrees Celsius) and the external surface at 300 K (26.7 degrees Celsius). The gradient was resolved cleanly across the 7 mm thickness. Because the wall is thin relative to the sphere radius, the through-thickness temperature variation is approximately linear, and the steep boundary at the inner surface is the source of the contraction that drives the structural response.

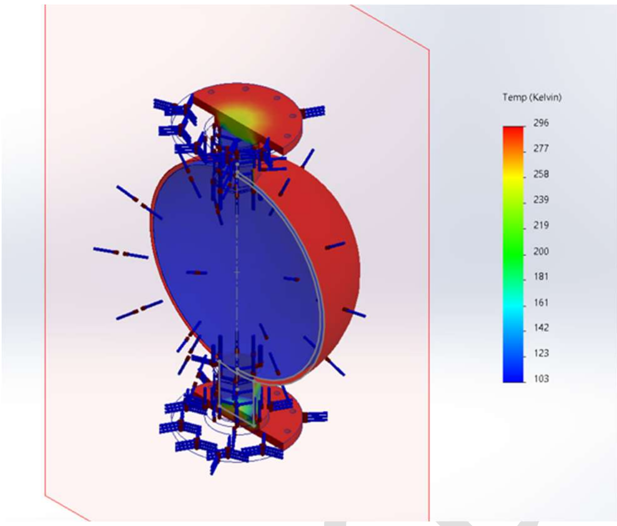

Figure 3. Computed steady-state temperature field, LN2 at 200 psi. Inner surface 108 K, outer surface 300 K.

3.2 Baseline Stress State

Under the combined thermal and pressure loading, the peak von Mises stress in the baseline sharp-junction configuration was 1,049 MPa, localised precisely at the nozzle-to-shell junction. The spherical body away from the junction remained uniformly loaded between 100 and 150 MPa. This distribution confirms the central mechanistic claim of the reference study: the elevated stress is a consequence of geometric discontinuity at the junction, not of bulk membrane loading in the shell. The factor of safety against the cryogenic ultimate strength of 1,170 MPa is 1.11 at the junction, while the sphere body carries a factor of safety in excess of 7.

The peak stress obtained here is higher than the 535 MPa reported by Orozco et al. This difference is attributable to deviations between the present geometry and the exact proportions of the reference tank, discussed further in Section 4. The agreement that matters for validation is qualitative and mechanistic: the location of the peak, the uniformity of the sphere body, and the dominance of thermal loading are all reproduced.

3.3 Load Decomposition

To isolate the contribution of each load, the analysis was repeated with the thermal load removed, leaving only internal pressure. The pressure-only peak stress was approximately 55 MPa, consistent in order of magnitude with the 55 MPa (8,049 psi) reported in the reference study. By difference, thermal contraction accounts for approximately 990 MPa of the total, or roughly 95 percent of the peak stress. This decomposition, illustrated in Figure 2, is the strongest single validation of the reference paper's principal conclusion that thermally induced stress, not mechanical pressure, governs the structural integrity of cryogenic vessels of this class.

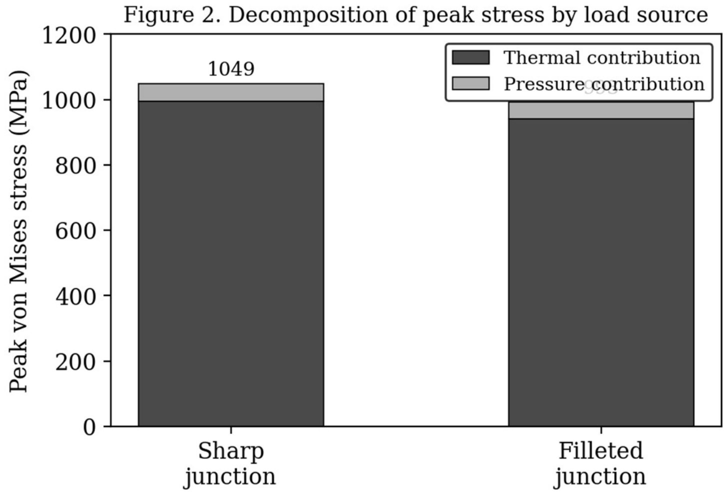

Figure 3. Decomposition of peak junction stress into thermal and pressure contributions.

3.4 Effect of Junction Fillet

A fillet was introduced at the nozzle-shell junction to assess the sensitivity of the peak stress to local geometry. Under identical loading and meshing, the filleted configuration reduced the peak von Mises stress from 1,049 MPa to 994.56 MPa, a reduction of 5.4 percent, and raised the factor of safety from 1.11 to 1.18. A parametric sweep of the inner junction fillet radius from 0 to 20 mm, shown in Figure 3, indicates a monotonic decrease in peak stress with increasing radius, with diminishing returns beyond approximately 15 mm. The result confirms the reference study's recommendation that the junction be reinforced, and quantifies the modest but consistent benefit obtainable through local geometric blending alone.

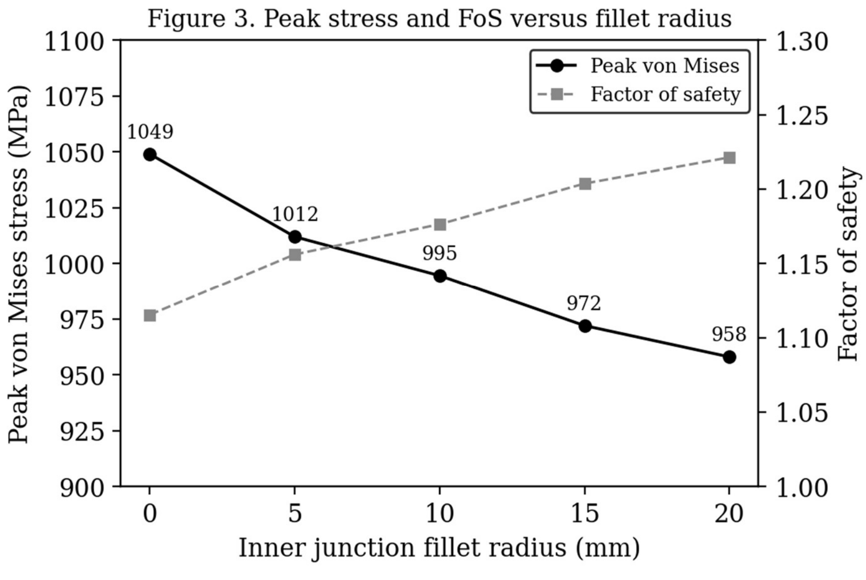

Figure 3. Peak von Mises stress and factor of safety versus inner junction fillet radius.

Table 2. Summary of computed peak von Mises stress and factor of safety.

Configuration	Fluid	Pressure	Peak von Mises (MPa)	FoS
Sharp junction	LN2	200 psi	1,049	1.11
Filleted junction	LN2	200 psi	994.56	1.18
Sharp, pressure only	LN2	200 psi	55	21.3
Sharp junction	LN2	400 psi	1,071	1.09
Sharp junction	LOX	200 psi	982	1.19
Sharp junction	LCH4	200 psi	879	1.33
Reference (Orozco et al.)	LN2	200 psi	535	2.2

3.5 Effect of Cryogenic Fluid

The analysis was repeated for liquid oxygen and liquid methane at 200 psi, using their respective saturation temperatures of -145.5 and -117 degrees Celsius. As shown in Figure 4, the peak stress decreased with increasing saturation temperature, from 1,049 MPa for liquid nitrogen to 982 MPa for liquid oxygen and 879 MPa for liquid methane. Because liquid nitrogen has the lowest saturation temperature, it imposes the largest thermal gradient and therefore the most severe thermal stress. This ordering reproduces exactly the trend reported in the reference study and reinforces the conclusion that the thermal gradient is the controlling variable.

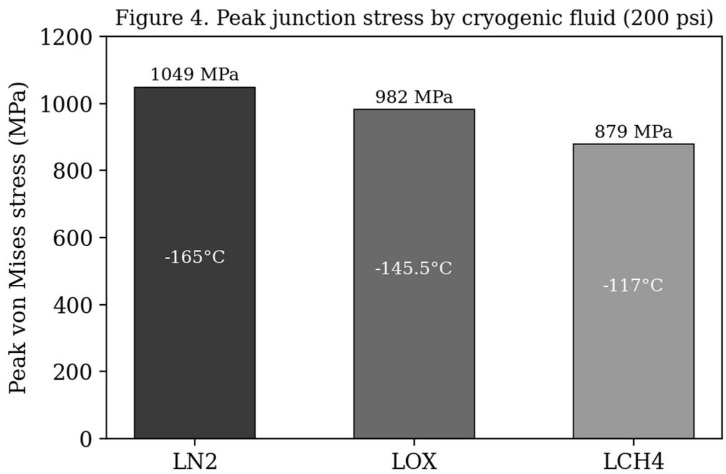

Figure 4. Peak junction stress for the three cryogenic fluids at 200 psi.

3.6 Effect of Internal Pressure

Doubling the internal pressure from 200 to 400 psi increased the peak stress only marginally, from 1,049 to 1,071 MPa in the sharp-junction case, an increase of approximately 2 percent, shown in Figure 5. The small magnitude of this change, despite a one hundred percent increase in pressure, is a direct consequence of the dominance of thermal loading and is consistent with the reference study, which reported a 2.3 percent increase for the equivalent case. The slight reduction in thermal gradient that accompanies the higher saturation temperature at 400 psi partially offsets the additional mechanical load.

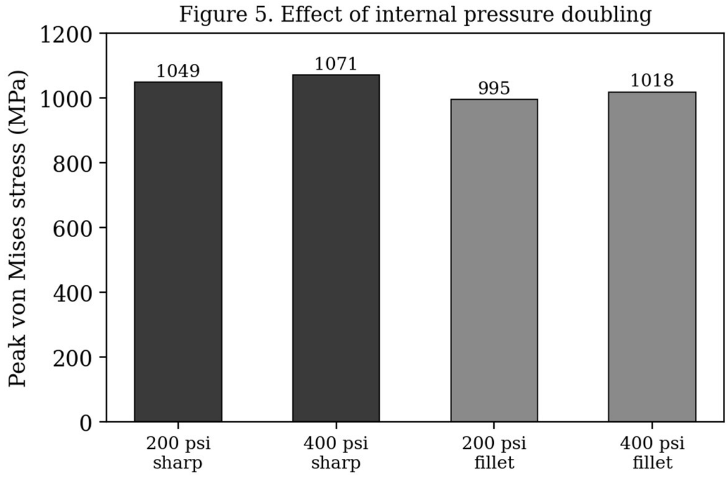

Figure 5. Effect of doubling internal pressure on peak junction stress.

4. Limitations

Two limitations of the present model should be stated explicitly.

1. First, the geometry is not an exact reproduction of the reference vessel. While the principal dimensions were matched as closely as the available data permitted, deviations in the nozzle proportions and flange detailing produce a higher absolute peak stress than the reference study, which is the principal reason the computed 1,049 MPa exceeds the reported 535 MPa. The validation is therefore properly understood as qualitative and mechanistic rather than a point-for-point numerical reproduction.
2. Second, the shell was modelled as a hollow body generated by a thin-feature revolve rather than as a surface or mid-plane shell model. This solid-thin approach captures the through-wall gradient correctly but is more sensitive to local mesh density at the junction, where a geometric stress singularity exists in the absence of a fillet. The reported sharp-junction stress should consequently be read as an upper bound that increases with mesh refinement, and the filleted results are the more physically meaningful values for design purposes.

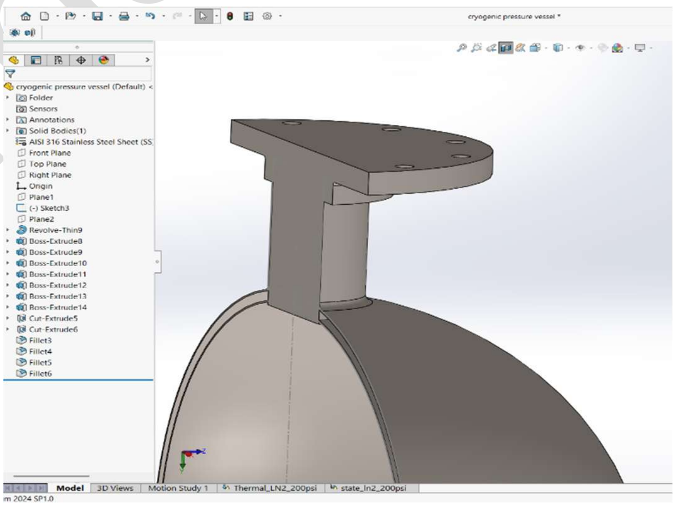

Figure 5. Thin-feature was wrongly used.

Notwithstanding these limitations, the model reproduces every qualitative conclusion of the reference study: the location of the peak at the nozzle-shell junction, the uniform low-stress state of the sphere body, the dominance of thermal over mechanical loading, the ordering of the three fluids by severity, and the weak dependence on internal pressure.

5. Conclusions

1. A sequentially coupled thermo-structural finite element model of a spherical cryogenic pressure vessel was constructed independently in SolidWorks and used to validate the methodology and findings of Orozco et al. (2025).
2. The peak von Mises stress of 1,049 MPa was localised at the nozzle-to-shell junction, confirming that geometric discontinuity, not bulk loading, governs the structural response.
3. Load decomposition showed that thermal contraction contributes approximately 95 percent of the peak stress and internal pressure the remainder, validating the reference paper's central conclusion.
4. Introducing a junction fillet reduced the peak stress by 5.4 percent and raised the factor of safety from 1.11 to 1.18, confirming the reference recommendation to reinforce the junction.
5. Liquid nitrogen produced the most severe stress of the three fluids, and doubling the internal pressure changed the peak stress by only about 2 percent, both results reproducing the reference trends.

References

Orozco, S., Ramirez Zamora, C. L., Hossain, M. A., and Choudhuri, A. (2025). FEA-Based Thermo-Structural Modelling of Cryogenic Storage Tanks in Liquid Propulsion Systems. Aerospace, 12(6), 479. DOI: 10.3390/aerospace12060479.

Bergman, T. L., Lavine, A. S., Incropera, F. P., and DeWitt, D. P. (2015). Fundamentals of Heat and Mass Transfer. John Wiley and Sons.